Day 1

Vector atomic gradiometer with laser-defined baseline

Wonjae Lee, Nezih Dural and <u>Michael Romalis</u>

Physics Department, Princeton University, Princeton NJ, USA

Vector magnetometry in Earth's field is often limited by angular rotation of the sensor's sensitive axes relative to the magnetic field vector. Angular rotation of the sensor by as little as 0.1 nanoradian is sufficient to generate several fT of false magnetic field reading. Using atomic gradiometry one can in principle cancel common sensor motion, but it requires very high stability of the relative alignment between the sensitive axes of the two sensors.

We describe a vector gradiometer that uses the direction of a probe laser beam to define a common sensitive axis for two magnetometer sensors. We demonstrate simultaneous detection of two transverse field gradients in Earth's size magnetic fields. The latest sensitivity measurements will be presented. Furthermore, we argue that the sensor has a unique property of being fundamentally limited by the longitudinal population relaxation time of the atoms, instead of the usual coherence relaxation time. We present experimental quantum noise measurements that set the fundamental limits of the sensitivity.

High-resolution magnetic field imaging at finite fields with a scalable Cs vapor cell

D. Hunter[1], C. Perrella[2], A. McWilliam[1], S. J. Ingleby[1], J. P. McGilligan[1], M. Mrozowski[1], P. F. Griffin[1], D. Burt[3], A. N. Luiten[2], and E. Riis[1]

[1]Department of Physics, SUPA, University of Strathclyde, Glasgow G4 0NG, UK
[2]Institute for Photonics and Advanced Sensing (IPAS), and School of Physical Sciences, University of Adelaide, SA 5005, Australia
[3]Kelvin Nanotechnology, University of Glasgow, Glasgow G12 8LS, UK

This work describes an optically pumped magnetometer (OPM) employing the free-induction-decay (FID) protocol [1], configured to provide high-resolution magnetic field imaging across the sensor area. An enhanced optical pumping strategy is implemented allowing consistent sensitivity performance ($< 200\,\mathrm{fT}/\sqrt{\mathrm{Hz}}$) over a broad dynamic range, providing a framework for precision sensing in unshielded environments. The sensor head comprises of a micro-machined cesium (Cs) vapor cell containing nitrogen (N_2) buffer gas as shown in Fig. 1(b). It was custom-built using novel fabrication techniques, enabling scalable and flexible geometries that can be tailored to accommodate various applications including magnetic imaging [2]. For example, vapor cells with a range of thicknesses up to $6\,\mathrm{mm}$ and cm-scale optical access can be fabricated. Their intrinsic spin relaxation properties are optimized based on the cell dimensions through precise tuning of the buffer gas content [3]. Close to unity spin polarization is generated by resonantly pumping the Cs D_2 line, maximizing signal amplitude and suppressing spin-exchange through light narrowing to reduce the transverse relaxation rate γ_2.
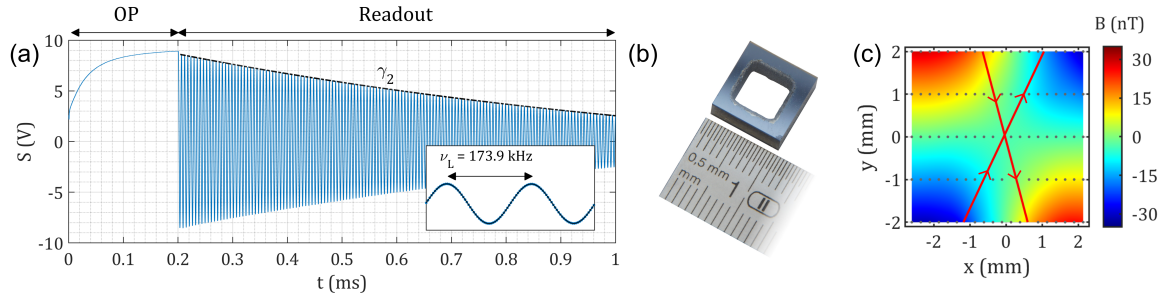

Figure 1: (a) FID OPM signal in a bias field of $B_0 \approx 50\,\mu\mathrm{T}$. (b) Sensor head based on a $3\,\mathrm{mm}$ thick Cs vapor cell containing N_2 buffer gas. (c) Magnetic image deviation from B_0 produced by a wire (red lines) placed in close proximity to the cell. The arrows indicate direction of current flow.

Locally independent measurements can be made within a single vapor cell due to the spatial confinement imposed by the buffer gas. This utility is explored in the context of magnetic field mapping with a FID-based sensor implementing a single pixel detection system [4]. Two-dimensional magnetic images are formed in a bias field of approximately $50\,\mu\mathrm{T}$, as seen in Fig. 1(c), by translating a $175\,\mu\mathrm{m}$ $(1/e^2)$ diameter probe beam. The spatial and temporal properties of a current oscillation are resolved up to the Nyquist limited bandwidth, extending the OPM's capabilities to imaging of kHz-level magnetic sources.

References

[1] D. Hunter *et al.*, Phys. Rev. Appl. **10**, 014002 (2018).
[2] S. Dyer *et al.*, J. Appl. Phys. **132**, 134401 (2022).
[3] S. Dyer *et al.*, arXiv:2304.06153 (preprint), (2023).
[4] D. Hunter *et al.*, arXiv:2303.10915 (preprint), (2023).

Atomic Vector Magnetometry Using Electromagnetically Induced Transparency

Y.J. Wang[1], I. Fan[1,2], Y. Li[1,2], M. Maldonado[3], I. Novikova[3], E. Mikhailov[3], J. McKelvy[4], A. Matsko[4], and J. Kitching[1]

[1]National Institute of Standards and Technology, Boulder, CO 80305, USA
[2] University of Colorado, Boulder, CO 80309, USA
[3] College of William & Mary, Willaimsburg, VA 23187, USA
[4] JPL, California Institute of Technology, Pasadena, CA 91109, USA

Scalar atomic magnetometers have shown high sensitivity at fT/ Hz$^{0.5}$ level [1,2]. Scalar magnetometer can be adapted to include measurement of magnetic field orientation but usually at the cost of accuracy. Magnetometry using electromagnetically induced transparency (EIT) can provide both scalar accuracy and vector information [3,4]. We present a scheme for magnetic field measurement with the common-mode drift suppression by probing multiple EIT resonances. The sensitivity has demonstrated to be 10 pT/ Hz$^{0.5}$ at 0.1 Hz and <200 pT/ Hz$^{0.5}$ at 1 mHz. The concept provides viable path toward a chip-scaled vector magnetometer [3].
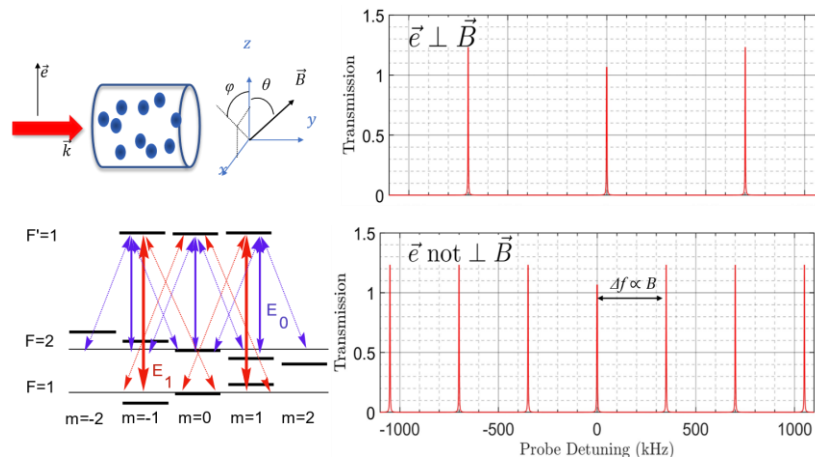
Figure 1: Concept of EIT vector magnetometer. The magnetic field strength is measured with frequency spacing of resonances and the orientation is extrapolated with relative amplitude.

References

[1] W. Clark Griffith *et al.*, "Femtotesla atomic magnetometry in a microfabricated vapor cell," *Opt. Express* 18, 27167-27172 (2010)

[2] I. Kominis *et al.*, "A subfemtotesla multichannel atomic magnetometer." *Nature* **422**, 596–599 (2003)

[3] V. I. Yudin *et al.*, "Vector magnetometry based on electromagnetically induced transparency in linearly polarized light." Physical Review A, 82(3), 033807-0338077 (2010)

[4] K. Cox, *et al.*, "Measurements of the magnetic field vector using multiple electromagnetically induced transparency resonances in Rb vapor." Physical Review A, 83(1), 015801 (2011).

[5] J. Kitching, "Chip-scale atomic devices", *Appl. Phys. Rev.*, 5, 031302 (2018).

Large-scale dual-chamber RF atomic magnetometer

K.L. Sauer[1], D. J. Heilman[1], N. Dural[2], D.W. Prescott[1], T.W. Kornack[3], C.Z. Motamedi[1], and M.V. Romalis[2]

[1]George Mason University, Fairfax, VA, USA
[2]Princeton University, Princeton, NJ, USA
[3]Twinleaf Inc., Princeton, NJ, USA

Preliminary results from one of the largest RF atomic magnetometer setups presently operating, shown in Fig. 1a, will be presented. The size of the magnetometer, 128 cm^3 in cell volume, with a correspondingly high number of ^{87}Rb atoms, can reduce spin-projection noise. In addition, multiple passes of the probe beam, 44 in total, are used to suppress photon-shot noise. The atoms are split between two-chambers to allow for opposite-helicity pumping of the atoms. In this gradiometer configuration, light-shift noise can also be cancelled.
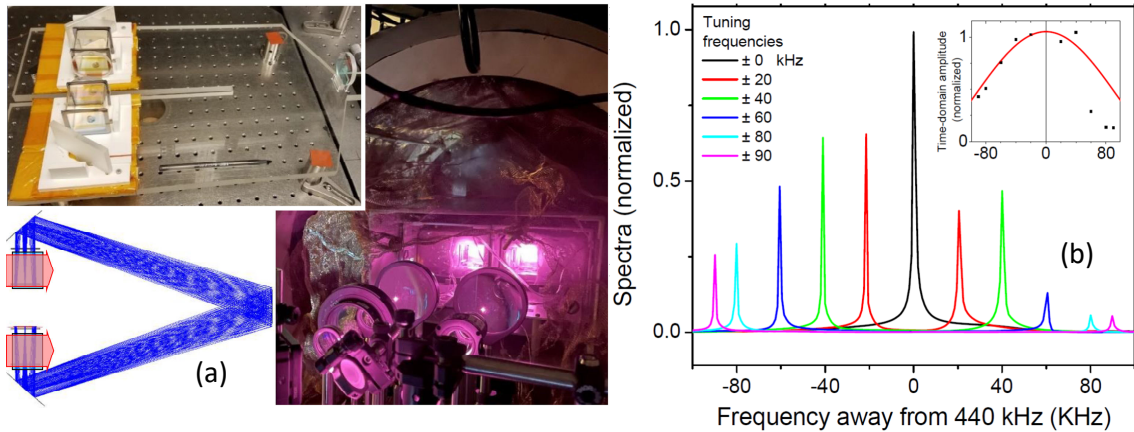

Figure 1: (1a) Large-scale RF magnetometer with two Rb cells (top inset) with multi-passes of the probe beam in a folded V-pattern (bottom inset) and pumped from the left with two separate pump beams (main graphic) with independent helicity. Each cell sits in its own separately controlled field coil. (1b) A single short strong pulse of 7 μs at 0.44 MHz, creates free-induction-decays in the two atomic cells which are measured simultaneously by the probe beam. Spectra with equal and opposite per-cell tuning fields are shown in the main graph. Part of the asymmetry around the center frequency is created by differing linewidths, but at the highest frequencies, signals are further suppressed due to self-shielding by the cells' ovens. This is apparent by looking at time-domain amplitudes compared to theory (red line), as shown in the inset.

The dual-chamber magnetometer can also be used to simultaneously measure two separate frequencies, using the same probe beam. One potential application of interest is the search for contraband material using nuclear quadrupole resonance, where the intrinsic quantum resonances of individual materials are virtually unique; e.g., potassium chlorate has a 0.53 MHz resonance, ammonium nitrate a 0.42 MHz one. Simultaneous measurement can significantly increase search speed. Each cell is placed in its own set of field coils, with both field coils nested inside of a larger set of field coils used to provide a common tuning field. An initial demonstration is shown in Fig. 2b.

Dual-axis Alkali-metal-noble-gas Comagnetometer with Pulsed Optical Pumping

J. Wang, J.Lee, H. Loughlin, M. Hedges, and M. V. Romalis[1]

[1]Department of Physics, Princeton University, Princeton, NJ, USA

Alkali-metal-noble-gas comagnetometers are precision probes well-suited for tests of fundamental physics and inertial rotation sensing, combining high sensitivity of the spin-exchange-relaxation free (SERF) magnetometers with inherent suppression of magnetic field noise. Past versions of the device utilizing continuous-wave optical pumping are sensitive to a single axis perpendicular to the plane spanned by the orthogonal pump and probe laser beams. These devices are susceptible to light shifts in the alkali atoms, and to power and beam pointing fluctuations of both the probe and pump lasers, the latter of which is a dominant source of $1/f$ noise. Here, we model and implement a new approach to alkali-metal-noble-gas comagnetometers using pulsed optical pumping. After each pump laser pulse, an off-resonance probe beam measures the precession of noble-gas-spins(n)-coupled alkali spins(e) via optical rotation in the dark, thus eliminating effects from pump laser light shift and power fluctuations. Performing non-linear fitting on the sinusoidal transient signal with a proper phase enables separate and simultaneous measurement of couplings along two orthogonal axes in the plane perpendicular to the pump beam. Effects from beam pointing fluctuations of the probe beam in the pump-probe plane is fundamentally eliminated, and signal response to pump beam pointing fluctuations is suppressed by compensation from n.[1]
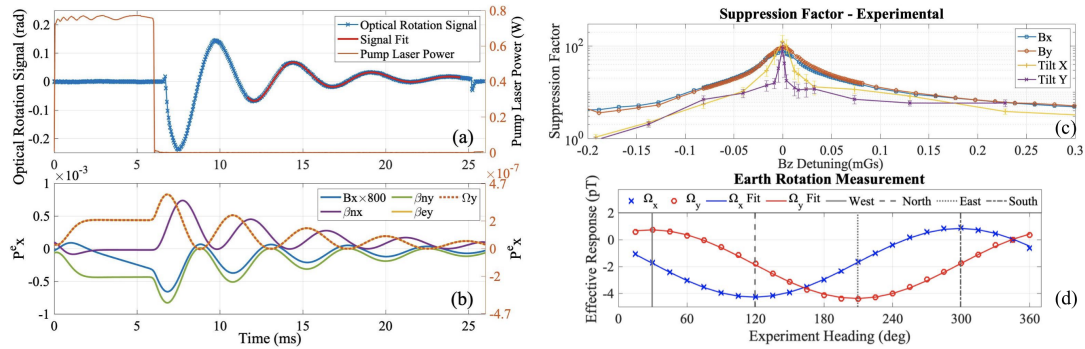
Figure 1: (a) Left: Experimental optical rotation signal for one pump period and its nonlinear fit. Right: Pump laser power. (b) Numerically simulated electron spin polarization along the comagnetometer's sensitive axis in response to 10^{-7} Gs of magnetic field B_x and anomalous fields β_{nx}, β_{ny}, β_{ey} (left), and to rotation $\Omega_y = 10^{-7}$ rad/s (right). (c) Suppression of transverse magnetic field and pump beam deflection around the operating bias field B_z. (d) Dual-axis angular velocity from earth's rotation measured simultaneously with the pulsed comagnetometer.

References

[1] Publication forthcoming.

Quantum-enhanced magnetometry at optimal number density

Charikleia Troullinou[1,2], Vito-Giovanni Lucivero[3], Morgan W. Mitchell[1,4]

[1]ICFO – The Institute of Photonic Sciences, Castelldefels (Barcelona), Spain
[2]Fraunhofer Centre for Applied Photonics, Glasgow, G1 1RD, UK
[3]Dipartimento Interateneo di Fisica,Universitá degli Studi di Bari Aldo Moro, Bari, Italy
[4]ICREA - Institució Catalana de Recerca i Estudis Avançats, 08010 Barcelona, Spain

Optical and atomic quantum noise in magnetometry can be reduced by optical squeezing and spin squeezing, respectively. As the atomic density of the OPM increases, the interplay between strong Faraday rotation and detrimental absorption and collisional effects determines the condition for optimal sensitivity.
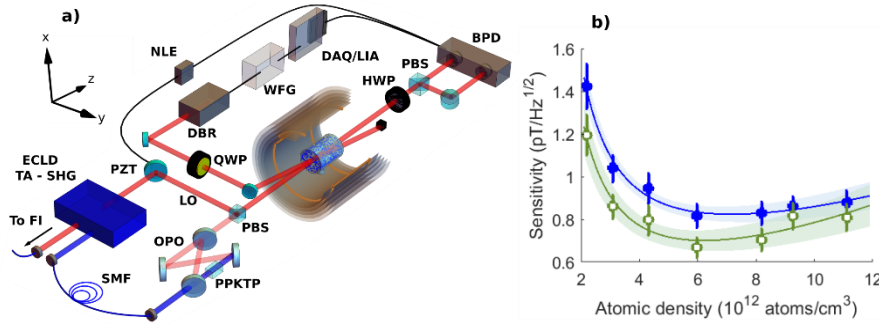
Figure 1: (a)Squeezed-light OPM experimental setup [1]. (b) The blue (green) data points indicate the OPM sensitivity versus atomic density measured at 500Hz for laser- (squeezed-) light probing. In agreement with the theoretical predictions (solid lines), quantum enhancement at optimal number density is observed.

We report **the use of squeezed probe light and evasion of measurement back-action to enhance the sensitivity and measurement bandwidth of a Bell-Bloom magnetometer with adjustable atom number density [2]**. By experimental observation, and in agreement with quantum noise modeling, a spin-exchange-limited OPM probed with laser light is shown to have an optimal sensitivity determined by density-dependent noise contributions. The application of squeezed probe light boosts the OPM sensitivity beyond this laser-light optimum, allowing the OPM to achieve sensitivities that it cannot otherwise reach.

References

[1] C. Troullinou, R. Jiménez-Martínez, J. Kong, V. G. Lucivero, and M. W. Mitchell, Phys. Rev. Lett. **127**, 193601 (2021)

[2] C. Troullinou, V. G. Lucivero and M. W. Mitchell, Submitted (2023)

Accurate Magnetic Field Extraction from FID Signals

D. Hewatt[1,2], M. Ellmeier[1], C. Kiehl[2], T. S. Menon[2], J. W. Pollock[1], S. Knappe[1,3], and C. A. Regal[2]

[1]*Mechanical Engineering, University of Colorado, Boulder, CO, USA*
[2]*JILA, National Institute of Standards and Technology and Department of Physics, University of Colorado, Boulder, CO, USA*
[3]*FieldLine Inc., Boulder, CO, USA*

We discuss how the accuracy of determining the magnetic field depends on the fitting method for a ^{87}Rb free induction decay (FID) magnetometer. Similar magnetometers use non-linear least squares methods to fit free precession signals to a single decaying cosine function. Our experiments and simulations show that, at lower optical pumping powers, FID signals cannot be accurately described by a single decaying cosine wave due to non-negligible contributions from atomic population in the F=1 manifold [1]. Additionally, the relative phase between the F=1 and F=2 hyperfine manifolds changes with pump power causing beating in the signal. These effects can reduce the accuracy of a single-frequency fit. In this presentation, we demonstrate a new fitting technique that uses a decaying cosine for each hyperfine manifold constrained by the Breit-Rabi formula. In systems where the pump power is limited, this fitting technique improves the accuracy, allowing us to reduce our fitting-based systematic bias to within 0.5 nT.
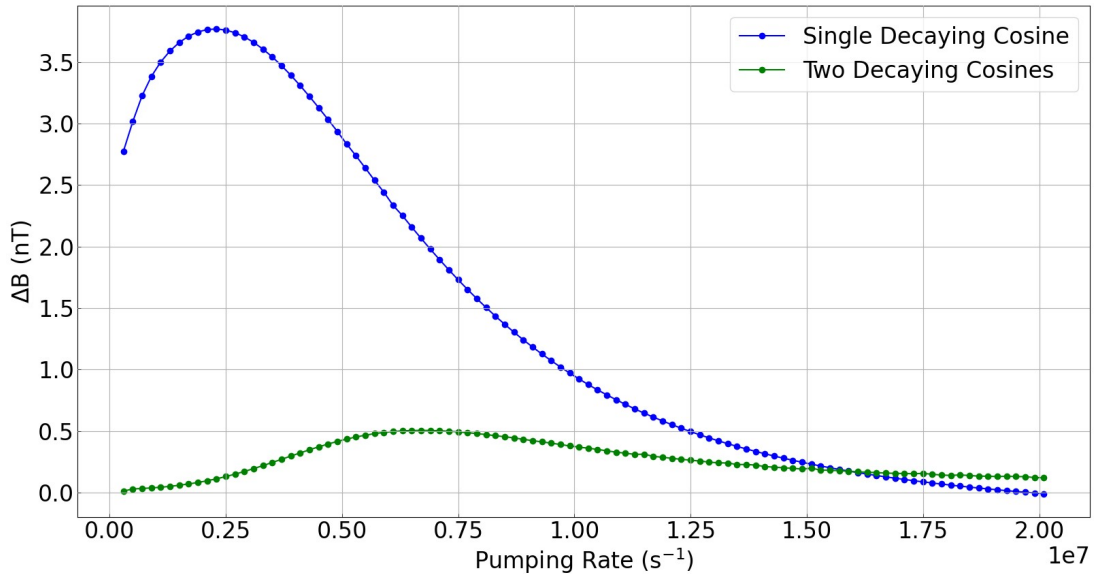
Figure 1: Density matrix simulation of magnetic field fitting error versus pumping rate. We show that fitting the FID signals to two decaying cosines (green dots) reduces the fitting error at lower pumping rates compared to a single decaying cosine (blue dots).

References

[1] W. Lee, V. G. Lucivero, M. V. Romalis, M. E. Limes, E. L. Foley, and T. W. Kornack Phys. Rev. A **103**, 063103 (2021).

Challenges for OPM in fundamental high-precision experiments

G. Bison[1] for the nEDM collaboration

[1]Paul Scherrer Institute, Villigen, Switzerland

Fundamental high-precision experiments often require controlling the magnetic environment in which they are performed. One such experiment is the new setup for neutron EDM searches at PSI. In this experiment both statistical and systematic uncertainties directly relate to inhomogeneities in the magnetic field. The installation includes a state-of-the-art active magnetic field suppression, a six-layer passive magnetic shield, optimized field coils inside the shield and two magnetometry systems based on 199Hg and 133 Cs. I will give an overview of how the systems were designed and implemented and report on the performance demonstrated so far. An important limiting factor is contamination with magnetic impurities which we characterize with a magnetic scanner derived from an OPM-based cardio magnetometer.
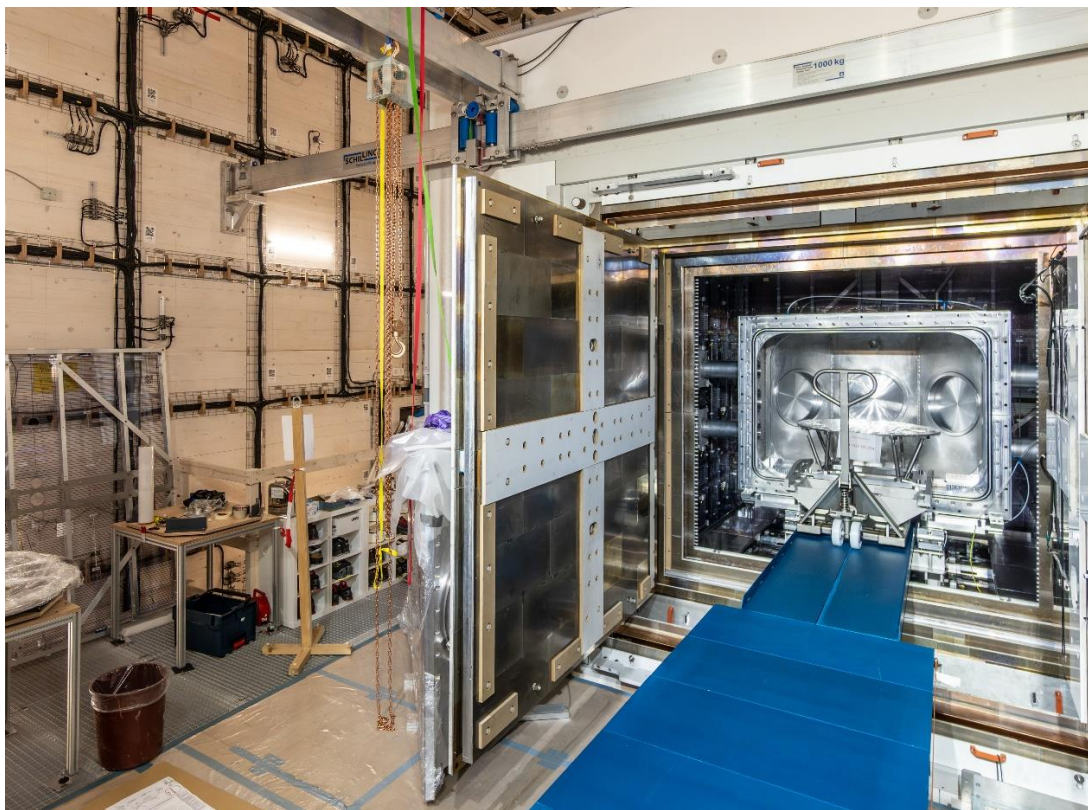

Figure 1: View into the experimental Area. The black cables are the coils for the active shield. The big door is one of three doors of the passive shield and the vacuum tank in the centre is surrounded by the field coil.

Sensitive magnetometer applications at Los Alamos

Igor Savukov and Young Jin Kim, Los Alamos National Laboratory, Los Alamos, NM, USA.

We have developed a number of sensitive magnetometers, including optically pumped multi-channel spin-exchange relaxation free (SERF), radiofrequency (RF), and adiabatic optical quantum sensors [1]. Among applications, we are focused on magnetoencephalography (MEG), magnetic resonance imaging (MRI), and applications in fundamental physics, such as axion searches. Currently, we are preparing compact multi-channel SERF magnetometers for MEG measurements. Also, we are developing high-sensitive RF magnetometers for axion searches in a large magnetic field. In my talk, I will give an overview of our work related to magnetometers. In some detail, I will describe recent new results. For example, I will present the adiabatic optical quantum sensor, which has advantage of unshielded operation and wide bandwidth, and the demonstration of improved MRI image quality at ultra-low field: 1x1 mm^2 in-plane resolution [2].

References:

[1] I. Savukov, Y. J. Kim, "Broadband Ultra-Sensitive Adiabatic Magnetometer," IEEE Sensors Applications Symposium (SAS) pp. 1-5 (2021).

[2] I Savukov, YJ Kim, S Newman, "High-resolution ultra-low field magnetic resonance imaging with a high-sensitivity sensing coil," Journal of Applied Physics 132 (17), 174503 (2022).

Precision measurement and spectroscopy with NV centers

V. M. Acosta[1]

[1]Deptartment of Physics & Astronomy, Center for High Technology Materials, University of New Mexico, Albuquerque USA.

Color centers in wide-bandgap semiconductors have emerged as a leading platform in the field of quantum sensing, broadly defined as the use of qubits to measure environmental parameters. In my lab at the University of New Mexico, we are using Nitrogen-Vacancy (NV) centers in diamond to image magnetic phenomena in condensed-matter and biological systems over a broad range of length scales. At the nanometer scale, we are building super resolution magnetic microscopes to image magnetic nanoparticles with 50-100 nm resolution. At the micrometer scale, we embed diamond sensors inside microfluidic chips to perform nuclear magnetic resonance spectroscopy at the scale of single cells [1]. At the millimeter scale, we use magnetic flux concentrators to detect femtotesla-level magnetic fields [2,3], with potential applications in medical imaging, navigation, and even dark matter detection [4]. I will provide an introduction to the field, discuss recent results and ongoing challenges, and outline future directions.

References

[1] J. Smits*, J. Damron*, P. Kehayias, A. F. McDowell, N. Mosavian, N. Ristoff, I. Fescenko. A. Laraoui, A. Jarmola, V. M. Acosta, **Science Advances** 5 eaaw7895 (2019)**.**

[2] I. Fescenko, A. Jarmola, I. Savukov, P. Kehayias, J. Smits, J. Damron, N. Ristoff, N. Mosavian, V. M. Acosta, **Physical Review Research** 2, 023394 (2020).

[3] Y. Silani, J. Smits, I. Fescenko, M. W. Malone, A. F. McDowell, A. Jarmola, P. Kehayias, B. Richards, N. Mosavian, N. Ristoff, V. M. Acosta, **Science Advances** 9 : eadh3189 (2023).

[4] P.-H. Chu*, N. Ristoff*, J. Smits, N. Jackson, Y. J. Kim, I. Savukov, V. M. Acosta, **Physical Review Research** 4, 023162 (2022).

Rydberg Atom-Based Sensors: Transforming Measurements and Detection of Radio-Frequency Fields and Communication Signals

Christopher L. Holloway, Alexandra B. Artusio-Glimpse, Andrew P. Rotunno, Nikunjkumar Prajapati, Samuel Berweger, and Matthew T. Simons

National Institute of Standards and Technology, Boulder, CO 80305, USA

One of the keys to developing new science and technologies is having sound metrology tools (i.e., measurement tools) and techniques. A stated goal of international metrology organizations, including the National Institute of Standards and Technology (NIST), is to make all measurements traceable to the International System of Units (SI). The world of measurement science is changing rapidly with the SI redefinition that occurred in 2018. As a result of the shift towards fundamental physical constants, the role of primary standards and measurements must change. Atom-based measurements allow for direct SI-traceable measurements, and as a result, measurement standards have evolved towards atom-based measurements over the last few decades- most notably length (m), frequency (Hz), and time (s) standards.

Recently, there has been great interest in extending this to magnetic and electric (E) field sensors. Fundamental to all electromagnetic/communication measurements is having accurately calibrated probes, antennas, and power meters in order to measure either E fields or power. In the past 10 years, we have made great progress in the development of a fundamentally new direct SI-traceable approach based on Rydberg atoms (traceable through Planck's constant, which is now an SI defined constant). Rydberg atom-based sensors now have the capability of measuring amplitude, polarization, and phase of the RF field. As such, various applications are beginning to emerge. These include SI-traceable E-field probes, power-sensors, voltage standards, receivers for communication signals (AM/FM modulated and digital phase modulation signals), and even RF camera and beam-profilers.

This new atom-based technology has allowed for interesting and unforeseen applications. In this talk, we will take a historical journey on the development of the Rydberg atom approach, and discuss various future applications and commercialization efforts.

Rydberg electrometry with multi-pass cells

Michael Romalis, Nezih Dural and Joe Wiedemann

Physics Department, Princeton University, Princeton NJ, USA

Electric field sensing with thermal Rydberg atoms provides a simple quantum platform for detection of weak microwave fields. The practical limitations of this technique are due to relatively weak optical transitions to the Rydberg state and several competing linewidth broadening mechanisms.

We describe our approach to Rydberg electrometry using multi-pass cells. In particular, we developed cells that allow different optical path lengths for the two overlapping and counter-propagating laser beams in a typical EIT setup. The multi-pass cells still allow free scanning of each laser frequency without standing waves. This approach allows us to optimize the optical density for the probe laser field and increase the transit time for the coupling laser beam. Furthermore, we use pulsed microwave and laser measurements to disentangle different relaxation mechanisms affecting Rydberg states, such as collisions with Cs and background gas atoms.

Detecting UHF-Band Electric Fields with Rydberg Atoms and Electromagnetically-Induced Transparency

M.A. Viray[1], B.N. Kayim[1], J.F. Jones[1], B.C. Sawyer[1], R. Wyllie[1],
S. Berweger[2], N. Prajapati[2], A.B. Artusio-Glimpse[2], A.P. Rotunno[2],
C.L. Holloway[2], M.T. Simons[2], E. Imhof[3], S.R. Jefferts[3],
J.M. Wheeler[3], and T.G. Walker[4]

[1]*Georgia Tech Institute of Technology, Atlanta, GA, USA*
[2]*National Institute of Standards and Technology, Boulder, CO, USA*
[3]*Northrop Grumman, Woodland Hills, CA, USA*
[4]*University of Wisconsin-Madison, Madison WI, USA*

We present results on Rydberg atom-based electric field sensing in the ultra high frequency (UHF) radio band. Rydberg atom-based electric field sensing is a burgeoning field of study that focuses on detecting radiation in the RF and microwave frequency bands. These incoming fields are detected by perturbing the Rydberg states, either resonantly or non-resonantly, and observing the atomic response. Resonant and non-resonant perturbations to the Rydberg state follow well-known physics, so by measuring the change in atomic response we can determine the incident field strength. In this work, we utilize a three-photon excitation scheme to excite rubidium-87 atoms in a vapor cell to Rydberg F-states. At these states, certain frequencies in the UHF band can resonantly drive $nF \rightarrow nG$ transitions. The magnitude of the UHF signals is then determined by monitoring the absorption of the probe laser (780 nm) through the vapor cell. The sensor's resonant frequency and sensitivity are a function of the principal quantum number n of the $nF \rightarrow nG$ transition; for $n = 45$, we report a sensitivity of 3.9 μV/(m$\sqrt{\text{Hz}}$) at a signal frequency of 899 MHz.
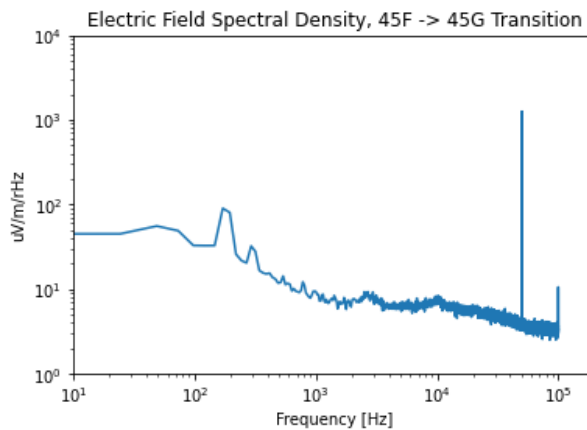
Figure 1: Power spectral density of a heterodyne beat note signal, scaled in units of electric field per $\sqrt{\text{Hz}}$. The heterodyne beat note frequency is 50 kHz, and the electric field sensitivity is determined from measuring the noise floor around the beat note frequency.

Day 2

A Vectorized Rb Magnetometer for CubeSat Missions

M. Ellmeier[1], D. Allison[3], T. Maydew[3], J. Hughes[3], C. Chism[2],

R. Marshall[2] and S. Knappe[1,3]

[1]*Dept. of Mechanical Engineering, University of Colorado, Boulder, USA*
[2]*Dept. of Aerospace Engineering Sciences, University of Colorado, Boulder, USA*
[3]*FieldLine Inc., Boulder, USA*

We develop a compact vector Rb magnetometer for a single 6U CubeSat spacecraft mission (COSMO) in LEO to provide scalar and vector magnetic field data for the World Magnetic Model. Therefore, the magnetometer must be able to measure Earth's magnetic field with an accuracy and precision less than or equal to 5 nT. To obtain all three vector components, a Mz magnetometer from FieldLine Inc. is mounted in a three-axis Braunbeck coil system and three slow varying modulation signals are applied to extract the FFT amplitudes. A calibration approach, similar as described in [1], corrects for the non-orthogonality of the coil system and extracts the modulation amplitudes β.
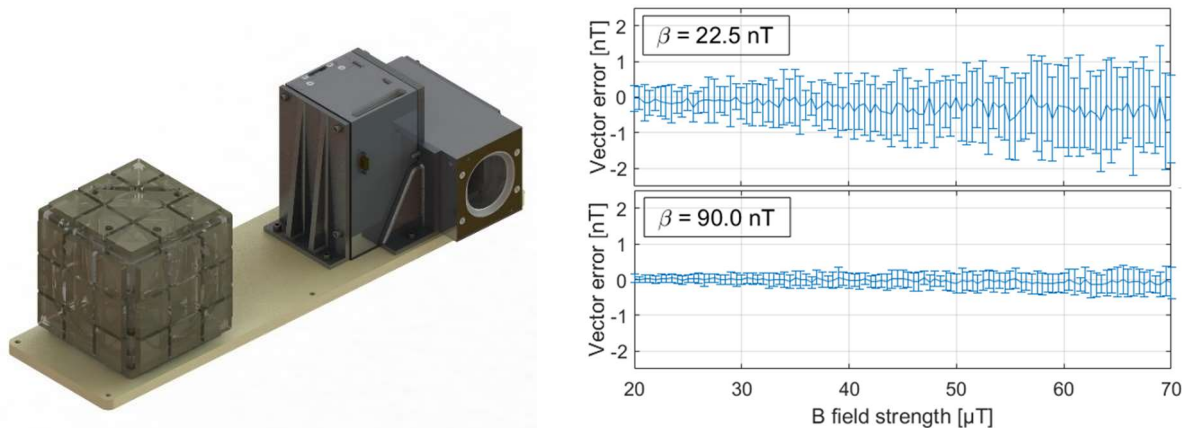

Figure 1: (left) Rendering of the satellite optical bench containing the Braunbeck system with the scalar magnetometer and two star trackers. (right) Simulation of the vector precision assuming a scalar noise level of 1 pT/√Hz for two different modulation amplitudes β.

Our vector precision is currently limited by the noise of the scalar magnetometer which is amplified by the ratio between the external magnetic field strength and the modulation amplitude. This ratio is optimized to obtain a vector precision below 1 nT. The main contributors to the vector accuracy are drifts of the modulation signals and temperature changes affecting the coil system. The presentation will outline our vectorization and calibration method as well as show accuracy and precision evaluation results of our first flight model.

References

[1] O. Gravrand, Earth, Planets and Space **53**, 949 (2001).

Decoding neural dynamics of face perception with optically pumped magnetometer magnetoencephalography

Wei Xu[1,2], Bingjiang Lyu[2], and Jia-Hong Gao[1,2]

[1]Academy for Advanced Interdisciplinary Studies, Peking University, Beijing, China
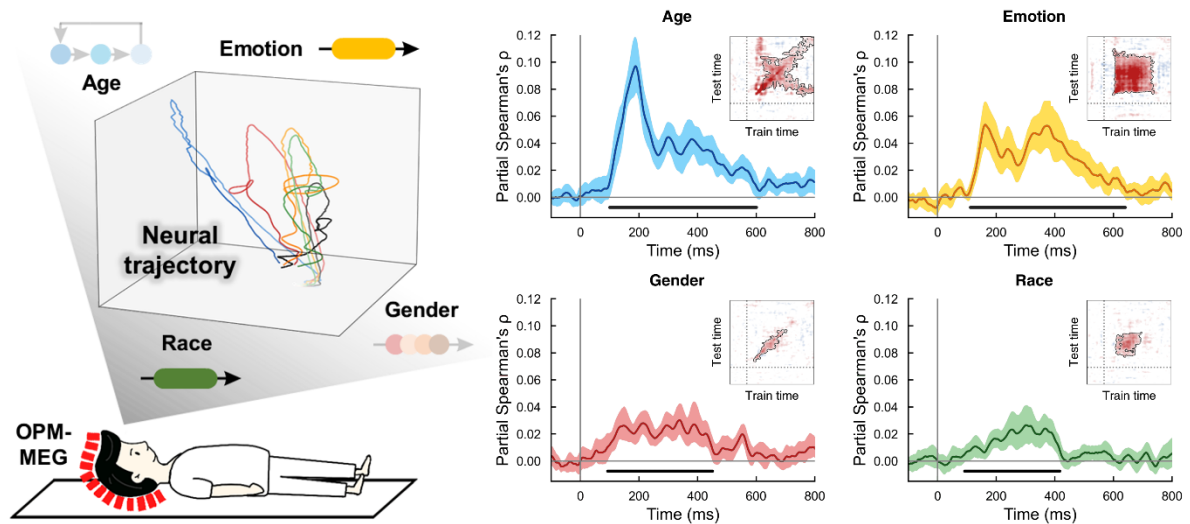*[2] Changping Laboratory, Beijing, China*

Figure 1: (Left) Neural representation trajectories of four dimensions of face stimuli. (Right) Temporal dynamics derived from SVM decoding results for each dimension with temporal generalization patterns at the upper right corner.

Optically pumped magnetometer magnetoencephalography (OPM-MEG) has advanced rapidly in recent years, overcoming the limitations of traditional SQUID-MEG and offering increased flexibility for studying human cognition. However, it remains unclear whether OPM-MEG is suitable to study higher cognitive processes. Here, using OPM-MEG, we systematically investigate the dynamic processing of various facial dimensions that are intricately intertwined in the brain. Our results reveal unique representation patterns of age, emotion, gender, and race, along with their temporal dynamics during face perception. Notably, we observed a significant sustained representation pattern for emotion and race evidenced by Bayesian model selection on temporal generalization patterns. Additionally, cross-domain generalization uncovers independent neural representations for each face dimension, further substantiating their unique neural profiles. Moreover, the neural trajectory is stretched when each face dimension is processed, with the length of trajectory corresponding to peak decoding accuracy of each face dimension. Taken together, our findings demonstrate, for the first time, the capability of OPM-MEG to decode the temporal dynamics and neural geometries that underlie face perception, providing novel insights into the processing of various face dimensions over time. Importantly, these decoding results exhibit high test-retest reliability across different sessions, highlighting the feasibility of utilizing OPM-MEG to explore the neural basis of higher-level human cognition in the future.

Multi-parameter quantum sensing and magnetic communications with a hybrid dc/rf optically-pumped magnetometer

M. Lipka[1], <u>A. Sierant</u>[2], C. Troullinou[2], and M. W. Mitchell[2,3]

[1]*Centre for Quantum Optical Technologies, Centre of New Technologies, University of Warsaw, Banacha 2c, 02-097 Warsaw, Poland*
[2]*ICFO - Institut de Ciencies Fotoniques, The Barcelona Institute of Science and Technology, 08860 Castelldefels (Barcelona), Spain*
[3]ICREA - Institucio Catalana de Recerca i Estudis Avancats, 08010 Barcelona, Spain

Optically-pumped magnetometers (OPMs) are paradigmatic quantum sensors that provide insight into quantum sensitivity limits and have applications in bio-medicine, space science and fundamental physics [1]. Multi-parameter quantum sensing [2] aims to extend quantum enhancement to simultaneous measurement of multiple physical parameters. Here we report an OPM capable of simultaneously measuring dc and rf fields with quantum-limited sub-pT/√Hz sensitivity (see Fig.1), making it a practical test-bed for quantum multi-parameter estimation (MPE). We demonstrate MPE-enabled spread spectrum magnetic communication, with possible application in ultra-compact radio receivers for communication underwater and underground.
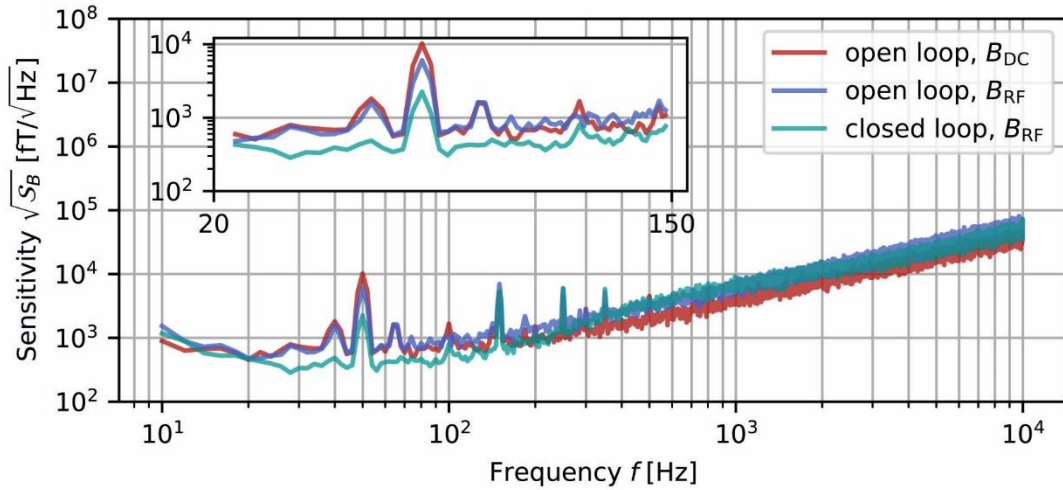
Figure 1: Sensitivity of the magnetometer for rf and dc operation with open or closed feedback loop.

References

[1] D. Budker and M. Romalis, Nature Physics **3**, 227 (2007).
[2] M. Szczykulska, T. Baumgratz, and A. Datta, Advances in Physics: X **1**, 621 (2016).

Rabi vector magnetometry

C. Kiehl[1] , T. S. Menon[1], T. Thiele[1], S. Knappe[2,3], C. A. Regal[1]

[1]*JILA, National Institute of Standards and Technology and University of Colorado, and Department of Physics, University of Colorado, Boulder, Colorado 80309, USA*
[2]*Mechanical Engineering, University of Colorado, Boulder, Colorado 80309, USA*
[3]*FieldLine Incorporated, Boulder, Colorado 80301, USA*

Many vector magnetometry applications, including magnetic anomaly detection, navigation, bio-imaging, and space exploration require vector accuracy. Here, we demonstrate an approach to accurate vector magnetometry that uses a set of microwave polarization ellipses (MPEs) as a 3D reference. An advantage of this technique is that independent information from Rabi oscillations can be utilized to extract both the magnetic field vector and drifts in MPE parameters to mitigate heading errors without recalibration. Futhermore, Rabi resonances between multiple hyperfine transitions enable accurate scalar evaluations to measure heading error in FID measurements.
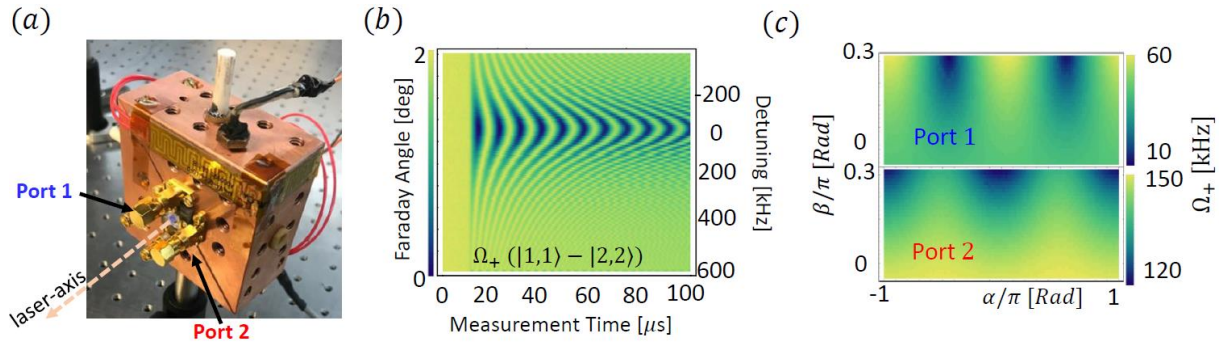
Figure 1: (a) Copper microwave cavity that generates MPEs. Port 1 and Port 2 excite near-degenerate modes of the cavity. (b) Chevron Rabi pattern of the σ^+ $|1,1\rangle - |2,2\rangle$ transition of Rb 87. (c) The dependence of the σ^+ Rabi frequency on the direction (α, β) of the ambient DC magnetic field for the two microwave cavity modes.

In this talk, I will discuss our implementation of this technique using a microfabricated vapor cell imbedded within a microwave cavity and present accuracy evaluations. By continuously sensing the Faraday rotation of a far-detuned probe bam, we record sequential Rabi frequencies every millisecond that enables sensitive vector measurements reaching down to 20 µRad/√Hz for geomagnetic-sized fields.

References

[1] T. Thiele, Y. Lin, M. O. Brown, and C. A. Regal, Phys. Rev. Lett. **121** 153202 (2018).

[2] C. Kiehl, D. Wagner, T. W. Hsu, S. Knappe, C. A. Regal, and T. Thiele, Phys. Rev. Res. **5**(1) L012002 (2023).

Two-Photon Atomic Magnetometry for Ultra-Low Frequency Electromagnetic Induction Imaging

Sidestepping the issue of bias field instability

in unshielded conditions

B. Maddox[1], and F. Renzoni[1]

[1] *University College London, Department of Physics & Astronomy, Gower St, London, UK*

The deployment of radio-frequency atomic magnetometers (RF-AMs) in electromagnetic induction imaging (EMI) offers the potential to outperform traditional induction coils, especially at ultra-low frequencies, where RF fields can penetrate common metals at super-mm length scales. To operate at such frequencies, the bias field is lowered to magnitudes that are comparable to typical fluctuations of the ambient urban magnetic field, and the RF-AM performance degrades, even with active magnetic compensation. Here we show that with the addition of a coupling RF field, two-photon RF transitions can give a resonance at ultra-low primary RF frequencies with an arbitrary bias field magnitude, which can be set much higher than the ambient magnetic field. We implement EMI with two-photon transitions in a portable unshielded RF-AM system, achieve stable resonances in the sub-kHz regime and demonstrate that the technique can detect features behind an Al shield of 3.2 mm which improves on our previous efforts by a factor of 8.
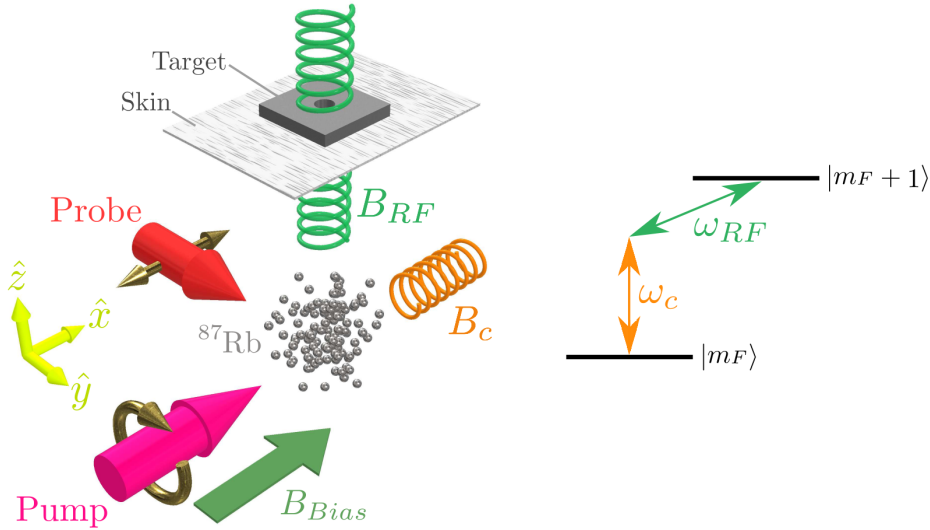
Figure 1: Illustrative depiction of the experimental geometry. A primary RF field B_{RF} and a coupling RF field B_c sum together to fulfil a two-photon transition between adjacent magnetic sublevels. The RF-AM is then sensitive to changes in the amplitude changes of B_{RF} as it penetrates the Al skin and induces eddy currents in the target.

References

[1] Maddox B, Renzoni F. *Two-photon electromagnetic induction imaging with an atomic magnetometer*. **Applied Physics Letters**. 122, no. 14 (2023).

Light shift effects in a Herriott-cavity-assisted scalar magnetometer using a single elliptically polarized beam

Ziping Xie[1] , Zengli Ba[2] and Dong Sheng[1]

[1]*Department of Precision Machinery and Precision Instrumentation,*
University of Science and Technology of China,
Hefei 230027, China
[2]*School of Physics, University of Science and Technology of China,*
Hefei 230026, China

A Herriott-cavity-assisted scalar magnetometer using a single detuned and elliptically polarized beam is built as shown in Fig. 1. The main problem in this magnetometer is the inherent light shift effect from the beam. Due to the complicated beam patterns inside the multiple-pass cavity, the atomic responses to the rf fields shows an asymmetric shape due to the light shift effect, which correlates with the beam detuning, beam polarization and bias field direction. An example of flipped line shapes for two opposite beam detunings are shown in Fig. 2. To suppress this effect, we add a half-wave plate at the center of the multipass cavity (inset of Fig. 2). The beam polarization flips each time when it passes the plate so that the light-shift effect can be spatially averaged out, and the symmetric line shape is recovered (red line in Fig. 2). In this way, this magnetometer provides an important alternative option to the commonly-used pump-probe scalar magnetometer with two beams. We will present the latest result of this magnetometer in this presentation.
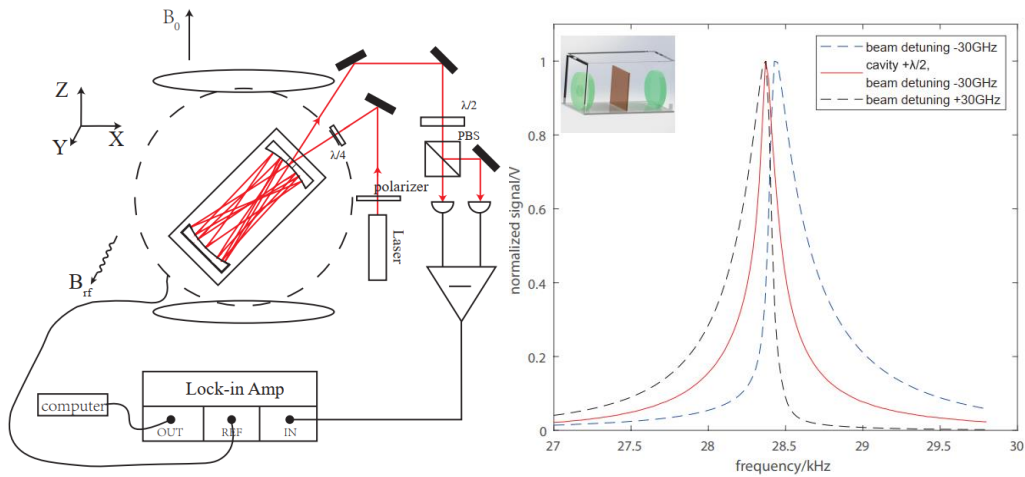

Fig.1 Schematic of the experimental apparatus.   Fig.2 Normalized demodulation signal.

Dedicated OPM Design for Magnetomyography

S. Nordenström[1], V. Lebedev[1], S. Hartwig[1], J. Marquetand[2,3], P. J. Broser[4], K. Vardhan[5], S. Neinert[5,6], M. Krutzik[5,6], and T. Middelmann[1]

[1]*Department of Biosignals, Physikalisch-Technische Bundesanstalt, Berlin, Germany*
[2]*Department of Neural Dynamics and Magnetoencephalography, Hertie-Institute for Clinical Brain Research, University of Tübingen, Tübingen, Germany*
[3]*MEG-Center, University of Tübingen, Tübingen, Germany*
[4]*Children's Hospital of Eastern Switzerland, St. Gallen, Switzerland*
[5]*Department of Physics, Humboldt-Universität zu Berlin, Berlin, Germany*
[6]*Ferdinand-Braun-Institut (FBH), Berlin, Germany*

Analysis of muscular activity is of key importance in diagnosing and investigating numerous neuromuscular diseases. However, needle electromyography (nEMG) is the current gold standard used by practitioners, which is an invasive and painful procedure. Optically pumped magnetometers (OPMs) employed for magnetomyography (MMG) might serve as a partial alternative to nEMG as they are non-invasive, sensitive, and miniaturizable. Moreover, OPMs can surpass the limitations of the non-invasive alternative to nEMG, surface EMG (sEMG) [1]. We have developed an OPM design especially suited for MMG. To enable measurements of rapid muscle signal components under harsh field conditions, our sensor design favors bandwidth, spatial resolution, and environmental field resilience, while maintaining sufficient sensitivity and partial directional information. We report on a lab-scale implementation of the design and show its potential for magnetic measurements of muscle activity. We compare the performance of our sensor to state-of-the-art commercial zero-field-OPMs operated in a compact magnetic shield as well as a magnetically shielded room. The high bandwidth of our OPM design might facilitate the detection of pathological traces in muscle signals not perceptible with commercial OPMs [2, 3], whereas its robustness makes its implementation outside of magnetically shielded rooms and future integration in clinical practice conceivable.

References

[1] T. Klotz et al., arXiv:2301.09494 (2023).

[2] P. J. Broser et al., Journal of Electromyography and Kinesiology **56**, 102490 (2021).

[3] J. Marquetand et al., Clinical Neurophysiology **132**, 2681-2684 (2023).

Bedside magnetocardiography with scalar OPM arrays

Geoffrey Z. Iwata, Christian T. Nguyen, Kevin Tharatt, Max Ruf, Tucker Reinhardt, Jordan Crivelli-Decker, Madelaine S.Z. Liddy, Alison E. Rugar, Frances Lu, <u>Ethan J. Pratt</u>, Kit Au-Yeung, Stefan Bogdanovic

SandboxAQ, Palo Alto, California USA

We designed and built a robust, bedside MCG device for deployment in practical settings. We utilized an array of scalar OPMs, in conjunction with custom noise rejection algorithms, to eliminate the need for magnetic shielding. This overcomes the chief barrier that currently prevents MCG devices from being widely adopted in clinical practice. We deployed this investigational MCG system in an office environment, in close proximity to operational roads, train tracks, and power lines. Demonstration of our device on healthy volunteers in several different usage conditions indicated that MCG images could be reliably acquired even when participants were not perfectly calm, compliant, and carefully pre-screened for magnetic objects. The work presented here heralds future deployments of our systems in bedside clinical settings, at the point of care for patients with acute coronary syndrome.
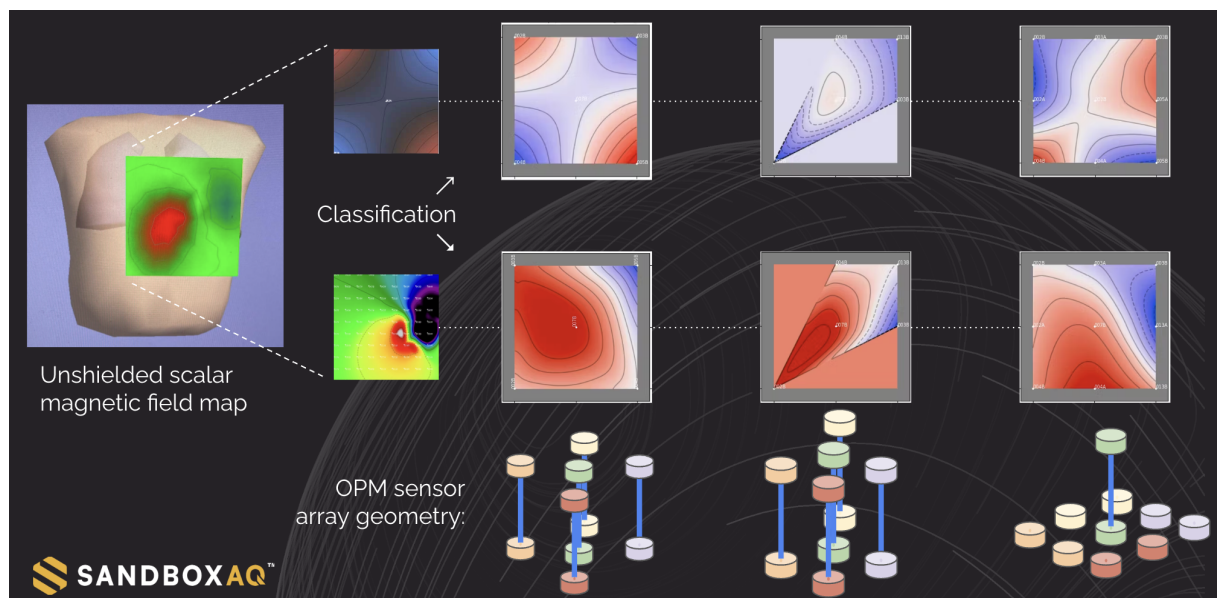
Figure 1: Magnetic field map images acquired with unshielded OPM sensor arrays.

References

[1] R. Fenici, R. Mashkar, and D. Brisinda, Eur. Heart J., vol. **41**, no. Supplement_2, p. ehaa946.0386, doi: 10.1093/ehjci/ehaa946.0386 (2020).

One, two or three: What is the optimum number of magnetic field components to measure in MEG?

L.M. Koponen[1]

[1]University of Birmingham, Birmingham, United Kingdom

Optically pumped magnetometers (OPMs) have, in many ways, challenged the conventional approach to magnetoencephalography (MEG). One promising avenue lies with vector MEG [1]. Unlike with conventional MEG with superconductive quantum interference devices and their superconductive pickup loops—where each additional B-field component requires a full new sensor—a single OPM vapour cell can be designed to measure up to all three B-field components—a vector OPM.

Even with OPMs, however, each additional B-field component comes with a small increase in sensor complexity and noise. Thus, the ability to measure all three components does not mean that they should always be measured. Rather, a simple theoretical argument [2] based on Shannon's information theory suggests that measuring just the normal component and its gradient should always outperform vector measurement (Fig. 1). Vector MEG experiments [1,3], however, indicate otherwise.

When the theory does not explain the experiments, the theory needs updating. In this work, I generalise the seminal channel capacity model [2] to include spatially correlated noise, which, unlike the uncorrelated noise, can be suppressed by the multichannel measurement. The generalised model provides further insight into the role of the two tangential B-field components, and their optimal sampling, such as which fraction of sensors should measure all three B-field components.
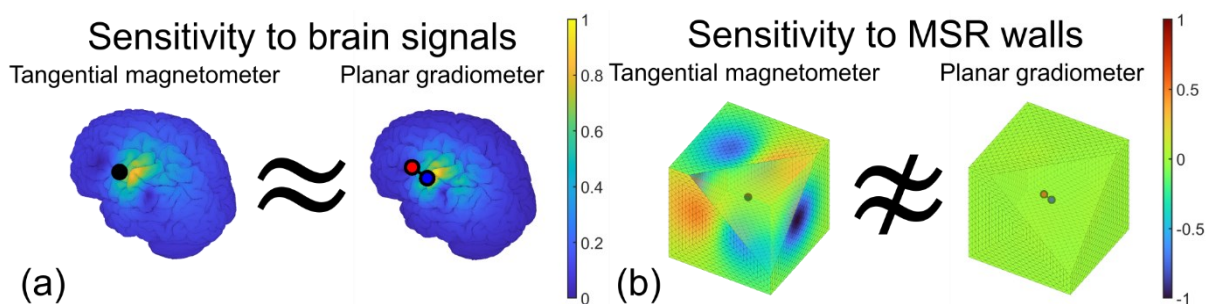

Figure 1: (a) For both intrinsic and synthetic gradiometers, for the brain signals, a planar gradiometer is almost indistinguishable from a tangential magnetometer. (b) But, compared to a gradiometer, a tangential magnetometer is far more sensitive to the spatially correlated external noise, allowing its measurement.

References

[1] M.J. Brookes et al., NeuroImage **236**, 118025 (2021).

[2] P.K. Kemppainen & R.J. Ilmoniemi, Advances in Biomagnetism, 635–638 (1989).

[3] M. Rea et al., Ann. N. Y. Acad. Sci. **1517**, 107–124 (2022).

Next Generation Acquisition and Control for OPM-MEG

H. Schofield[1,2], **R. M. Hill[1,2]**, **E. Boto[2,1]**, **M. J. Brookes[1,2]**, **J. Osborne[3]**, **C. Doyle[3]**, **V. Shah[3]**

[1]University of Nottingham, Nottingham, UK, [2] Cerca Magnetics Ltd., Nottingham, UK, [3]QuSpin, Louisville CO, USA

Introduction: Optically pumped magnetometers (OPMs) have revolutionised neuroimaging, enabling a new generation of MEG system which allows movement during scanning. However, most existing OPM-arrays require complex cabling to control each OPM, making ambulatory motion challenging. Here we trial a new OPM array design with miniaturised control and data acquisition electronics integrated into a wearable "backpack". We compare system performance to an established OPM-MEG system and determine its viability for MEG measurements.

Methods: The system comprised 64 triaxial OPMs (QuSpin) (192 independent MEG channels) mounted in a 3D printed helmet (Cerca Magnetics Ltd). The OPMs are connected to a miniaturised digital control electronics and data acquisition system (QuSpin) housed inside a backpack. Data from each OPM are transferred to a data acquisition box via ethernet connection. The electronics can be positioned a maximum of 80 cm from the OPMs. Firstly, noise recordings were taken in an empty magnetically shielded room (Magnetic Shields Ltd.). We contrasted this with an established system comprising 57 triaxial OPMs each controlled by its own electronics [1]. Then, we measured MEG signals from an individual performing a button press task. Data were processed by a beamformer to generate functional images depicting the spatial signature of beta modulation.

Results: Noise spectra are shown in Figure 1C. For both systems, the noise floors were 15 fT/sqrt(Hz) or lower. The presence of the system electronics in close proximity to the sensors had little effect on system noise. Figure 1D shows beta modulation induced by a button press, with primary effects in sensorimotor cortex and the expected oscillatory signature (movement induced beta desynchronisation followed by a post movement rebound) clearly delineated.

Discussion: Our results show clearly that the new system is capable of collecting high quality MEG data. Minimised cabling means new opportunities for ambulatory experimentation – which is of interest for studying neurodevelopment and movement disorders. The removal of long cabling to electronics outside the MSR means the system is less vulnerable to electronic interference.
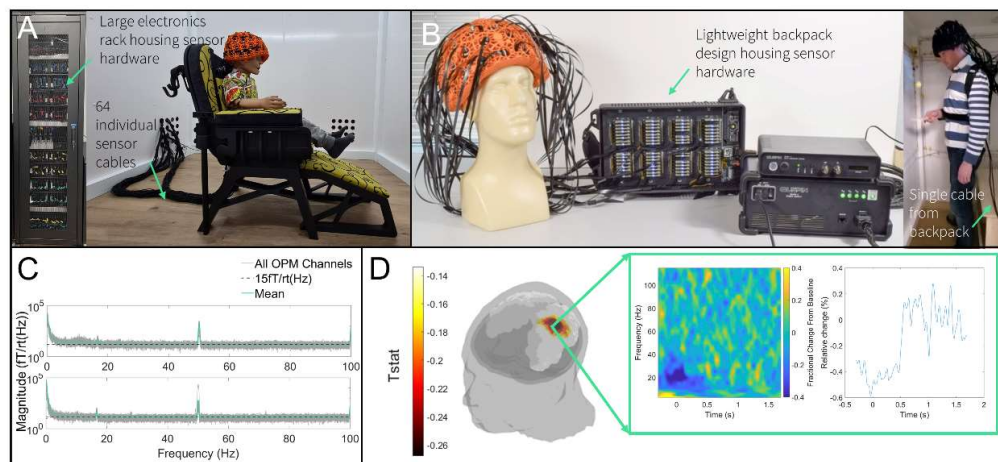

Figure 1: A) Current state of the art OPM-MEG system set-up. B) New backpack design. C) Noise spectra (top: new system, bottom: current system). D) Tstat image and time frequency spectrogram showing results from the button press task.

References

1.   Rhodes, N., et al., *Measurement of Frontal Midline Theta Oscillations using OPM-MEG.* NeuroImage, 2023. **271**: p. 120024.

Unshielded magnetoencephalography in an office environment

**T. Kornack, E. Foley, L. Rathbun, D. Newby, M. Limes,
D. Murray, N. Ford, A. Nelson, B. Miley, [1]
S. McBride, A. Braun,[2]
W. Lee, M. Romalis,[3]
T. Cheung[4]**

[1] *Twinleaf LLC, Plainsboro, USA*
[1] *SRI International, Princeton, USA*
[3] *Princeton University, Princeton, USA*
[4] *Simon Fraser University, Burnaby, Canada*

Figure 1: Magnetoencephalography recording in an office with windows.

We will discuss progress towards biomagnetic measurements in an office environment using total field gradiomoeters similar to [1].

References

[1] Phys. Rev. Applied 14, 011002 (2020).

Localization of OPM sensors with large electromagnetic coils

<u>M. Grön</u>[1], E. Luostarinen[1], M. Henttonen[1], S. Lauronen[1], O. Ahola[1], C. Pfeiffer[1], L. Parkkonen[1]

[1]Aalto University, Department of Neuroscience and Biomedical Engineering, Espoo, Finland

To estimate cortical signal sources from MEG recordings, the position and orientation of the OPM sensors must be known. Here we address this need by localizing OPMs with position-encoded magnetic fields generated by the same electromagnetic coils employed in field nulling [1].

In our OPM-MEG system, we have computer-controlled biplanar coils around the measurement volume [2,3,4]. These coils generate the three homogenous and the five independent first-order gradients of the field within a target volume of 20-cm radius. However, the accuracy of these fields is not sufficient for sensor localization. Following the approach of Iivanainen and colleagues [1], we measured with a fluxgate (Mag-03MC1000, Bartington Instruments Ltd, Whitney, UK) the fields generated by our coils at 48 equispaced locations and modelled them with vector spherical harmonic functions. We considered the space inside a 30x30x20-cm³ cuboid; the fit error was 2–25%. With the modelled coil fields, we then estimated the position and orientation of the x-, y- and z-channels of the fluxgate separately, i.e. the fluxgate channels have independent positions; the average localization error was 1.6 cm and 1.3° (Fig. 1). We expect that increasing the field-sampling SNR and shrinking the target volume will reduce the localization error considerably to a level acceptable for MEG source estimation.
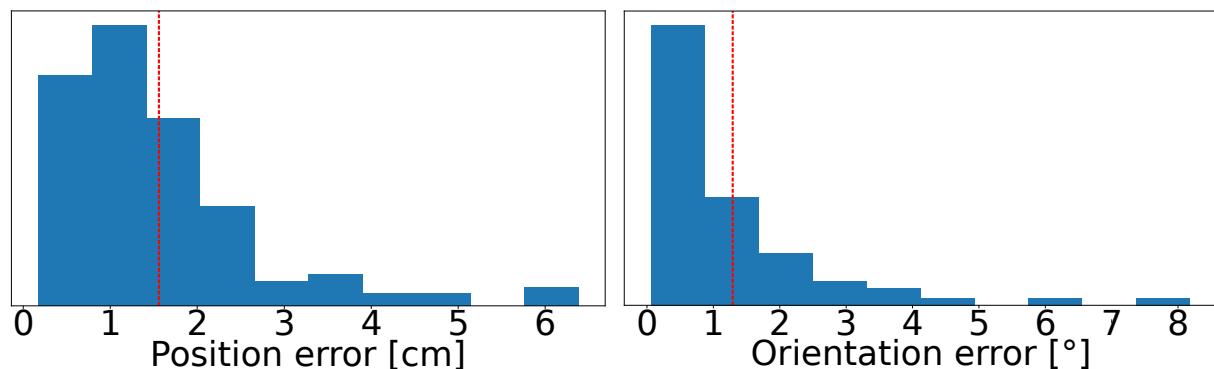

Figure 1: Localization error when localizing the x-, y- and z-channels of a fluxgate, i.e. the fluxgate channels have independent positions, in a 30x30x20-cm³ cuboid at 48 equispaced locations. (Left) Position error (mean: 1.6 cm). (Right) orientation error (mean: 1.3°).

References

[1]   J. Iivanainen et al., Sensors 22(8), 3059 (2022).
[2]   J. Iivanainen et al., Neuroimage 194, p.244-258 (2019).
[3]   A. Mäkinen et al. Journal of Applied Physics, 128(6), p.063906 (2020).
[4]   R. Zetter et al. Journal of Applied Physics, 128(6), p.063905 (2020).

Digital frequency estimation in self-oscillating OPM for high-precision portable DC magnetometry

Aurélien Chopinaud[1], M. Mrozowski[1], D. Hunter[1], P. F. Griffin[1], E. Riis[1] and S. J. Ingleby[1]

[1] *Dpt. of Physics, SUPA, University of Strathclyde, 107 Rottenrow, Glasgow, UK*

Finite-field optical magnetometry offers practical advantages in geomagnetic measurement due to the dynamic range, sensitivity and accuracy achievable with alkali double-resonance techniques. Resonant modulation at the Larmor frequency is applied to the alkali spins in order to drive the atomic response [1]. Greater signal-to-noise ratio and bandwidth can be achieved by running this system as a self-oscillating spin maser where a feedback loop spontaneously generates oscillation of the atoms at the Larmor frequency [2]. Precise determination of the Larmor frequency allows the detection of small and fast variations of geomagnetic fields. In order to utilise this method in a real-life environment it must be compact and fully portable, ideally to fit in a backpack or on a drone, and for this reason we focus on techniques that can be ported to the architecture of an embedded processor, such as a field-programmable gate array (FPGA).
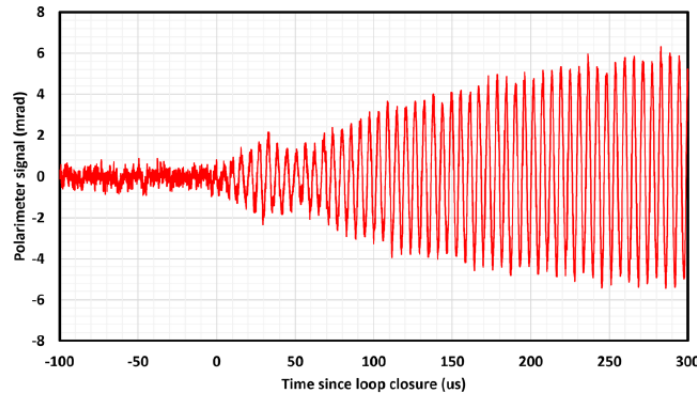

Figure 1: Digital spin maser response following closure of feedback loop at t = 0 s in a static field of $50\ \mu T$ [5].

Here we take advantage of a Hilbert transform routine implemented on dual finite-impulse response (FIR) filters [5], allowing real-time estimation of the spin maser signal phase at each clock cycle [3], and hence reconstruct the time-evolution of the magnetic field. We test our approach and characterise its full capacity on a shielded laboratory double-resonance spin-maser system using an anti-relaxation-coated ^{133}Cs cell [4], as well as develop its field implementation using a microfabricated alkali vapour cell and chip-scale laser, yielding a portable device [5]. We discuss the range of applications for this technology, including resilient positioning systems and high-resolution study of space weather.

References

[1] I. M. Savukov et al., Phys. Rev, Lett. **95,** 063004 (2005)

[2] W. Chalupczak and P. Josephs-Franks, Phys. Rev, Lett. **115**, 033004 (2015)

[3] N. Wilson et al., Phys. Rev. Res. **2**, 013213 (2020)

[4] N. Castagna et al., Appl. Phys. B **96**, 763-772 (2009)

[5] S. Ingleby et al., Sci. Rep. **12,** 12888 (2022)